Statistical analysis

All measurements are expressed as the mean ± S.E.M. (standard error of the mean). Overall differences between the groups were determined by one-way analysis of variance (one-way ANOVA). When the one-way ANOVA results were significant for 3 samples, the differences between each group were estimated using the Tukey–Kramer test. Simple comparisons of the mean and S.E.M. of the data were performed using the Student's *t*-test. The differences were considered to be significant at $P < 0.05$.

Results

Kinetics of gene expression induced by US and NBs

To investigate the kinetics of transgene transfection in the TA muscle induced by the US/NB method, bioluminescence imaging was performed (Fig. 1). Luciferase activity was detectable when pGL3 + US were administered but the combination of pGL3 + US + NBs showed an enhanced luciferase activity on each day ($P < 0.01$). The luciferase gene expression reached a peak 4 d after transfection. These results demonstrate the transient nature of US/NB-mediated gene transfer.

Cotransfection with pGL3 and hNIS genes in the TA muscle

Transgene expression was analyzed by RT-PCR 48 h after US/NB-mediated cotransfection of

pGL3 and hNIS. Figure 2 demonstrates that both transgenes were co-expressed in the same TA muscle.

Biodistribution of ^{124}I

To confirm the disposition of ^{124}I in mice and to determine whether the NIS expression detected by RT-PCR resulted in the expression of a functional protein, TA muscles of BALB/c mice were cotransfected with pGL3 and hNIS using the US/NB method, while saline solution was injected into the right TA muscle as a control. For most organs and tissues, the accumulation of ^{124}I reached its maximum value at 60 min, and decreased at 180 min (Fig. 3). The highest accumulation of ^{124}I was in the thyroid, and the lowest accumulation was in the brain. There was significant accumulation of ^{124}I at 60 min ($P < 0.05$) and 180 min ($P < 0.01$) in the TA muscle transfected with hNIS compared to the control TA muscle. These data suggest that the transfection procedure results in the synthesis of an active protein. In addition, we demonstrate here that US/NB-mediated transfection is restricted to the site of US administration as no ectopic NIS-mediated iodide accumulation was detected.

Blocking of ^{124}I in the TA muscle

To confirm that the ^{124}I accumulation observed in the TA muscle was indeed due to the expression of NIS, we used autoradiography to determine the accumulation of ^{124}I in the TA muscle, in the presence or absence of a large excess of cold iodide. Figure 4B shows that the

accumulation of ^{124}I (Fig. 4A) was completely blocked by the injection of non-radioactive NaI (Fig. 4B).

Visualization of gene expression

To determine whether the NIS expression detected on biopsies (by RT-PCR (Fig. 2), biodistribution (Fig. 3), and autoradiography (Fig. 4)) could also be detected by PET imaging. BALB/c mice were subjected to US/NB-mediated gene transfer (day 0) and subjected to bioluminescence imaging on day 3 and PET imaging (Fig. 5). The data presented in Figure 5 show a specific signal in the transfected TA muscle (left muscle), while no signal was observed in the right muscle injected with saline. Autoradiographic analysis performed on muscle biopsies confirmed the PET imaging results (Fig. 5A). These data, obtained with "normal" BALB/c mice were repeated on mice suffering from arthritis and vasculitis disease (Fig. 5B), and muscular dystrophy model mice (Fig. 5C) with very similar results.

Discussion

Ultrasound and nano/microbubbles have been developed for applications in experimental therapeutics. In gene therapy, this methodology has been exploited to increase the infectivity of adeno-associated viruses *(24)*, adenoviruses *(25)*, and retroviruses *(26)*. In addition, US/NB-mediated gene transfer has been used in non-viral approaches to deliver plasmid

DNA to experimental tumors *(27)*, the pancreas *(28)*, to antigen-presenting cells *(29)*, and the kidneys *(30)*.

Skeletal muscle is a key target for many gene therapy applications, including peripheral ischemia, secreted protein production, cancer and infection vaccines, and Duchenne muscular dystrophy *(31)*. In this context, our results demonstrate that the US/NB gene transfer technology is very effective. Considering the low toxicity, ease of use, and flexibility of this methodology, US/NB-mediated gene transfer should be considered as the method of choice for the TA muscle. We also demonstrated that the signal is transient and reaches a peak 4 d after transfection (Fig. 1). Our results are in agreement with another recent report, demonstrating that muscle is more amenable to US/NB-mediated gene transfer than subcutaneous or orthotropic tumors *(32)*. In addition, we demonstrated that gene transfer mediated by US and NB can also be performed on arthritic mice or mice suffering from muscle degeneration, suggesting that these pathologies do not impair the transduction potential of the methodology.

We cotransfected pGL3 and hNIS into the TA muscle using the US/NB method (Figs. 2, 3, 4, and 5). This cotransfection method is based on the hypothesis that two plasmids have the same backbone and promoter. The promoter of pGL3 is the Simian virus 40 (SV40), while that of the hNIS gene is the cytomegalovirus (CMV). It has been reported that the gene

expression levels differed (SV40 < CMV) when plasmids with the SV40 and CMV promoter both expressed the same gene product *(33)*. So et al. showed a correlation between the ^{125}I uptake of the hNIS gene and the bioluminescence activity induced by the luciferase gene when a plasmid with both the luciferase and hNIS genes was transfected *in vitro (34)*. Therefore, it is reasonable to select mice and to visualize the gene expression of hNIS using PET based on the expression of the luciferase gene. In addition, Figure 2 clearly showed that both genes were expressed after cotransfection in the TA muscle. Extrapolated to a physiopathological situation and based on these data, it is possible to envisage therapeutic strategies combining the action of at least two transgenes carried by different expression plasmids. This flexibility may provide the means for a "mix-and-match approach" to provide optimal therapeutic efficiency.

The biodistribution study was important to confirm the radiation exposure before PET imaging. Figure 3 demonstrates that specific accumulation of ^{124}I was observed in the thyroid and stomach when endogenous NIS was expressed *(35)*, and in the bladder as a result of iodide excretion *(36)*. Low levels of ^{124}I accumulation were observed in the brain, indicating that iodide does not pass the blood–brain barrier *(37)*. In addition, we demonstrated that US/NB-mediated transfection is restricted to the site of US administration as no ectopic NIS-mediated iodide accumulation was detected in sites not subjected to the

transfection procedure. These results are agreement with a previous ^{125}I study that suggested ^{124}I is available as well as ^{125}I *(38)*. In addition, the radioiodide activity of the TA muscle transfected with the hNIS gene indicated a twofold accumulation compared to the control TA muscle. This result demonstrates that the specific accumulation of ^{124}I in the TA muscle occurred by the ectopic expression of the hNIS gene. Since accumulation of ^{124}I in the blood was observed until 180 min, the residual ^{124}I internal exposure should be investigated in a future study.

To confirm the specific binding of ^{124}I in mouse TA muscle, we injected non-radioactive NaI before administration of ^{124}I (Fig. 4). The uptake of ^{124}I was blocked by NaI, indicating that hNIS was actually transfected in the TA muscle. The results of the biodistribution and blocking studies showed that the hNIS gene was transfected in the TA muscle by the US/NB method and the accumulation of ^{124}I was due to its expression.

In this study, we verified the effectiveness of gene delivery using the US/NB method and the visualization of gene expression using PET towards the development of gene therapy. Expression of the hNIS gene was confirmed at the peak of gene transfer determined by bioluminescence imaging. However, longitudinal studies are required for this to be applicable as a clinical endpoint. We administered ^{124}I (74MBq i.v.) for PET imaging (Fig. 5). This dose is ten times larger than used in previous studies *(39)* and is similar to that used in a

clinical study *(40)*. Acute radiation injury in mice will occur at this dose and longitudinal studies are not possible under these conditions. We administered this amount of dose for the following reasons: (1) this was the first study using 124I and Fine-PET, (2) the sensitivity of the Fine-PET is 40 cps/kBq/mL (*17*) (one tenth of that of the commercially available micro-PET imaging system). In future studies, we will conduct a longitudinal analysis of gene expression with a lower injected dose of ^{124}I.

Conclusion

This study demonstrates for the first time the proof of principle that PET imaging can be used to visualize US/NB-mediated gene transfer. This technology provides a new platform to detect non-viral-mediated gene transfer and, extrapolated to patients, a new clinical endpoint for future clinical trials that may include patients suffering from genetic disorders (i.e., vascular diseases and muscular dystrophy). In this perspective, we are developing a new plasmid that combines a therapeutic gene and the hNIS gene to visualize the therapeutic effect; we are also improving the US/NB-hNIS/PET system to improve the levels of transfection and expression.

Acknowledgements

Y. Watanabe received a Grant-in-Aid for JSPS Fellows (21-7073). S. Horie received a Grant-in-Aid for JSPS Fellows (21-7271). C. Rui received a Grant-in-Aid for Scientific Research for JSPS Postdoctoral fellowship For Foreign Researchers (P09127). S. Mori received a Grant-in-Aid for Scientific Research (B) (19390507). T. Kodama received a Grant-in-Aid for Scientific Research (B) (20300173); Grant-in-Aid for Exploratory Research (21650124); Grant-in-Aid for Scientific Research on Priority Area, MEXT (17012002, 18014002, 20015005); Grant for Research on Advanced Medical Technology, Ministry of Health, Labor, and Welfare of Japan (H19-nano-010); Grant for Research for Promotiong Technological Seeds (03-017); and Japan-France Integrated Action Program (SAKURA) Joint Project.

Figure legends

Figure 1. Peak of gene expression in mouse TA muscle

Kinetics of luciferase gene expression in the TA muscles by the US/NB method. (A) Luciferase activity after transfection. (B) Bioluminescence imaging. pGL3 + US (n = 3), pGL3 + US + NB (n = 4). The bars represent the mean ±S.E.M. $P < 0.01$ (**).

Figure 2. RNA isolation and RT-PCR for luciferase and NIS

Gel electrophoretic analysis of an RT-PCR reaction for luciferase and/or hNIS expression in mice TA muscle induced by NBs and US. Lane M: 0.1–2 kbp size ladder. Lane 1: β-actin (739 bp), Lane 2: Luciferase (689 bp), Lane 3: hNIS (581 bp).

Figure 3. Biodistribution of ^{124}I

pGL3 and hNIS were cotransfected into the left TA muscle of BALB/c mice using the US/NB method, while saline solution was injected into the right TA muscle as a control. The distribution of ^{124}I (370 kBq) is observed 30 (thyroid: $n = 1$, the others $n = 4$), 60 ($n = 6$), and 180 (thyroid: $n = 3$, the others: $n = 4$,) min after the injection. The radioactivity of the tissues was expressed as the percentage of the injected dose per gram (%ID/g). The bars represent the mean ± S.E.M. $P < 0.01$ (**) and $P < 0.05$ (*).

Figure 4. Blocking ^{124}I in the TA muscle

Autoradiography localization of ^{124}I in mouse TA muscle axial slices. Mice cotransfected with pGL3 and hNIS were divided into 2 groups 4 d after transfection. (A) One group was i.v. injected with $Na^{124}I$ (1.85 MBq) and scarified 2 h later. (B) The other group was i.p. injected with NaI. After 15 min, $Na^{124}I$ (1.85 MBq) was i.v. injected and the group was scarified 2 h later. The color bar shows logarithmic radioactivity.

Figure 5. Visualization of gene expression

We used three types of mice: control (A); arthritis and vasculitis disease (B); and muscular dystrophy model mice (C). In all images, the left TA muscle (L) was cotransfected with pGL3 and hNIS by the US/NB method, while the right TA muscle (R) was injected with saline. In all images, upper show the Bioluminescence image on 3 d after transfection, middle show PET images on 4 d after transfection ($Na^{124}I$ 74 MBq i.v.), and bottom show Autoradiography of the TA sections. Radioactive tracer accumulated in the left TA section, while it did not accumulate in the right TA section. The color bar shows logarithmic radioactivity.

References

1. Edelstein ML, Abedi MR, Wixon J, Edelstein RM. Gene therapy clinical trials worldwide 1989-2004-an overview. *J Gene Med.* 2004;6:597-602.
2. Penuelas I, Mazzolini G, Boan JF, et al. Positron emission tomography imaging of adenoviral-mediated transgene expression in liver cancer patients. *Gastroenterology.* 2005;128:1787-1795.
3. Bekeredjian R, Chen S, Frenkel PA, Grayburn PA, Shohet RV. Ultrasound-targeted microbubble destruction can repeatedly direct highly specific plasmid expression to the heart. *Circulation.* 2003;108:1022-1026.
4. Inubushi M, Tamaki N. Radionuclide reporter gene imaging for cardiac gene therapy. *Eur J Nucl Med Mol Imaging.* 2007;34 (Suppl 1):S27-33.
5. Watanabe Y, Aoi A, Horie S, et al. Low-intensity ultrasound and microbubbles enhance the antitumor effect of cisplatin. *Cancer Sci.* 2008;99:2525-2531.
6. Aoi A, Watanabe Y, Mori S, Takahashi M, Vassaux G, Kodama T. Herpes simplex virus thymidine kinase-mediated suicide gene therapy using nano/microbubbles and ultrasound. *Ultrasound Med. Biol.* 2008;34:425-434.
7. Chen R, Chiba M, Mori S, Fukumoto M, Kodama T. Periodontal gene transfer by ultrasound and nano/microbubbles. *J. Dent. Res.* 2009;88:1008-1013.
8. Kodama T, Tomita Y, Watanabe Y, Koshiyama K, Yano T, Fujikawa S. Cavitation Bubbles Mediated Molecular Delivery During Sonoporation. *J. Biomech. Sci. Eng.* 2009;4:124-140.
9. Weissleder R, Pittet MJ. Imaging in the era of molecular oncology. *Nature.* 2008;452:580-589.
10. Chen RF, Li ZH, Pan QH, et al. In vivo radioiodide imaging and treatment of pancreatic cancer xenografts after MUC1 promoter-driven expression of the human sodium-iodide symporter. *Pancreatology.* 2007;7:505-513.
11. Dai G, Levy O, Carrasco N. Cloning and characterization of the thyroid iodide transporter. *Nature.* 1996;379:458-460.
12. Yeom CJ, Chung JK, Kang JH, et al. Visualization of hypoxia-inducible factor-1 transcriptional activation in C6 glioma using luciferase and sodium iodide symporter genes. *J. Nucl. Med.* 2008;49:1489-1497.
13. Groot-Wassink T, Aboagye EO, Wang Y, Lemoine NR, Reader AJ, Vassaux G. Quantitative imaging of Na/I symporter transgene expression using positron emission tomography in the living animal. *Mol Ther.* 2004;9:436-442.
14. Fortin MA, Salnikov AV, Nestor M, Heldin NE, Rubin K, Lundqvist H.

Immuno-PET of undifferentiated thyroid carcinoma with radioiodine-labelled antibody cMAb U36: application to antibody tumour uptake studies. *Eur J Nucl Med Mol Imaging.* 2007;34:1376-1387.

15. Barton KN, Stricker H, Brown SL, et al. Phase I study of noninvasive imaging of adenovirus-mediated gene expression in the human prostate. *Mol Ther.* 2008;16:1761-1769.

16. Tai YC, Ruangma A, Rowland D, et al. Performance evaluation of the microPET focus: a third-generation microPET scanner dedicated to animal imaging. *J. Nucl. Med.* 2005;46:455-463.

17. Ishii K, Kikuchi Y, Matsuyama S, et al. First achievement of less than 1 mm FWHM resolution in practical semiconductor animal PET scanner. *Nucl Instrum Meth A* 2007;576:435-440.

18. Chisholm EJ, Vassaux G, Martin-Duque P, et al. Cancer-specific transgene expression mediated by systemic injection of nanoparticles. *Cancer Res.* 2009;69:2655-2662.

19. Mori S, Tanda N, Ito MR, et al. Novel recombinant congenic mouse strain developing arthritis with enthesopathy. *Pathol. Int.* 2008;58:407-414.

20. Huang M, Batra RK, Kogai T, et al. Ectopic expression of the thyroperoxidase gene augments radioiodide uptake and retention mediated by the sodium iodide symporter in non-small cell lung cancer. *Cancer Gene Thera.* 2001;8:612-618.

21. Glaser M, Mackay DB, Ranicar ASO, Waters SL, Brady F, Luthra SK. Improved targetry and production of iodine-124 for PET studies. *Radiochim acta.* 2004;92:951-956.

22. Yamazaki H, Ishii K, Funaki Y, et al. Production of "No Carrier Added" Iodine-124 from a Reusable Enriched Tellurium-124 Dioxide Target and its Application to an Ultra-High Resolution Animal PET Study. [Proceedings] *16th Pacific Basin Nuclear Conference.* 2008:P16P1299.

23. Kanai Y, Yamazaki H, Funaki Y, et al. Radiosynthesis of [124I] iomazenil and imaging of rat brain by means of semiconductor high resolution animal PET scanner. [Meeting Abstracts] *J. Nucl. Med.* 2008 ;49:308P-b-.

24. Li HL, Zheng XZ, Wang HP, Li F, Wu Y, Du LF. Ultrasound-targeted microbubble destruction enhances AAV-mediated gene transfection in human RPE cells in vitro and rat retina in vivo. *Gene Ther.* 2009;16:1146-1153.

25. Howard CM, Forsberg F, Minimo C, Liu JB, Merton DA, Claudio PP. Ultrasound guided site specific gene delivery system using adenoviral vectors and commercial ultrasound contrast agents. *J. Cell. Physiol.* 2006;209:413-421.

26. Taylor SL, Rahim AA, Bush NL, Bamber JC, Porter CD. Targeted retroviral gene delivery using ultrasound. *J Gene Med.* 2007;9:77-87.
27. Hayashi S, Mizuno M, Yoshida J, Nakao A. Effect of sonoporation on cationic liposome-mediated IFNbeta gene therapy for metastatic hepatic tumors of murine colon cancer. *Cancer Gene Ther.* 2009;16:638-643.
28. Chai R, Chen S, Ding J, Grayburn PA. Efficient, glucose responsive and islet-specific transgene expression by a modified rat insulin promoter. *Gene Therapy.* 2009;16:1202-1209.
29. Un K, Kawakami S, Suzuki R, Maruyama K, Yamashita F, Hashida M. Enhanced transfection efficiency into macrophages and dendritic cells by the combination method using mannosylated lipoplexes and Bubble liposomes with ultrasound exposure. *Hum Gene Ther.* 2010;21:65-74.
30. Xing Y, Pua EC, Lu X, Zhong P. Low-amplitude ultrasound enhances hydrodynamic-based gene delivery to rat kidney. *Biochem. Biophys. Res. Commun.* 2009;386:217-222.
31. Braun S. Muscular gene transfer using nonviral vectors. *Curr Gene Ther.* 2008;8:391-405.
32. Tsai KC, Liao ZK, Yang SJ, et al. Differences in gene expression between sonoporation in tumor and in muscle. *J Gene Med.* 2009;10:933-940.
33. Yang JP, Huang L. Direct gene transfer to mouse melanoma by intratumor injection of free DNA. *Gene Ther. 1996*;3:542-548.
34. So MK, Kang JH, Chung JK, et al. In vivo imaging of retinoic acid receptor activity using a sodium/iodide symporter and luciferase dual imaging reporter gene. *Mol Imaging.* 2004;3:163-171.
35. Spitzweg C, Joba W, Eisenmenger W, Heufelder AE. Analysis of human sodium iodide symporter gene expression in extrathyroidal tissues and cloning of its complementary deoxyribonucleic acids from salivary gland, mammary gland, and gastric mucosa. *J. Clin. Endocrinol. Metab.*1998;83:1746-1751.
36. Dwyer RM, Bergert ER, O'Connor MK, Gendler SJ, Morris JC. Sodium iodide symporter-mediated radioiodide imaging and therapy of ovarian tumor xenografts in mice. *Gene Ther.* 2006;13:60-66.
37. Hwang do W, Kang JH, Chang YS, et al. Development of a dual membrane protein reporter system using sodium iodide symporter and mutant dopamine D2 receptor transgenes. *J. Nucl. Med.* 2007;48:588-595.
38. Groot-Wassink T, Aboagye EO, Glaser M, Lemoine NR, Vassaux G. Adenovirus biodistribution and noninvasive imaging of gene expression in vivo by positron

emission tomography using human sodium/iodide symporter as reporter gene. *Hum Gene Ther.* 2002;13:1723-1735.

39. Pandey SK, Sajjad M, Chen Y, et al. Comparative positron-emission tomography (PET) imaging and phototherapeutic potential of 124I- labeled methyl-3-(1'-iodobenzyloxyethyl)pyropheophorbide-a vs the corresponding glucose and galactose conjugates. *J. Med. Chem.* 2009;52:445-455.

40. Phan HT, Jager PL, Paans AM, et al. The diagnostic value of 124I-PET in patients with differentiated thyroid cancer. *Eur J Nucl Med Mol Imaging.* 2008;35:958-965.

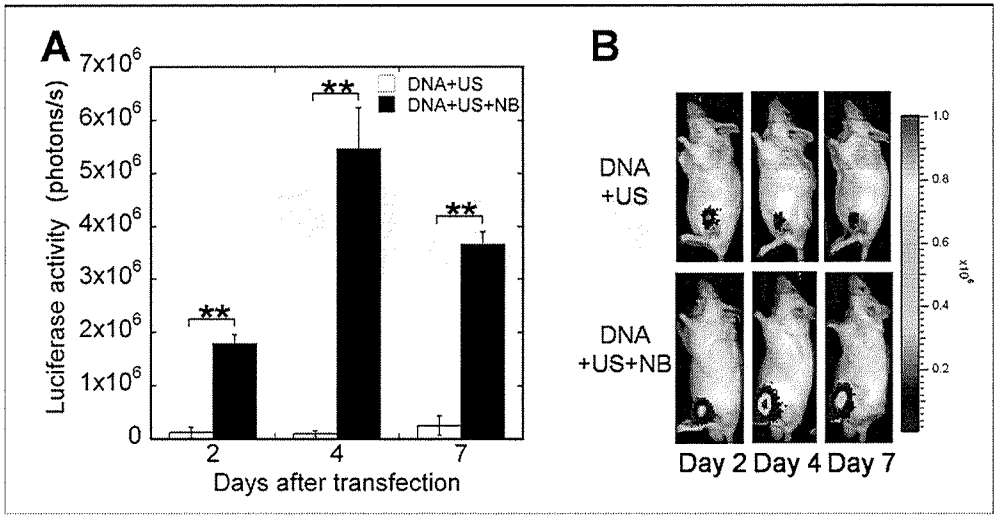
A
Luciferase activity (photons/s)
7x10^6
6x10^6
5x10^6
4x10^6
3x10^6
2x10^6
1x10^6
0
DNA+US
DNA+US+NB
**
**
**
2
4
7
Days after transfection
B
DNA
+US
DNA
+US+NB
1.0
0.8
0.6
0.4
0.2
x10^6
Day 2 Day 4 Day 7

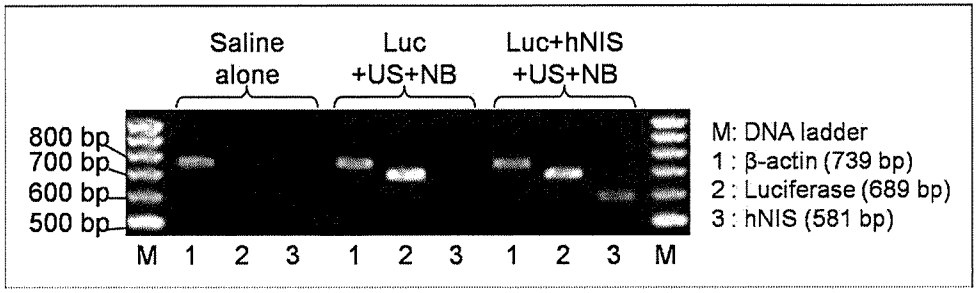
Saline
alone
Luc
+US+NB
Luc+hNIS
+US+NB
800 bp
700 bp
600 bp
500 bp
M 1 2 3 1 2 3 1 2 3 M
M: DNA ladder
1 : β-actin (739 bp)
2 : Luciferase (689 bp)
3 : hNIS (581 bp)

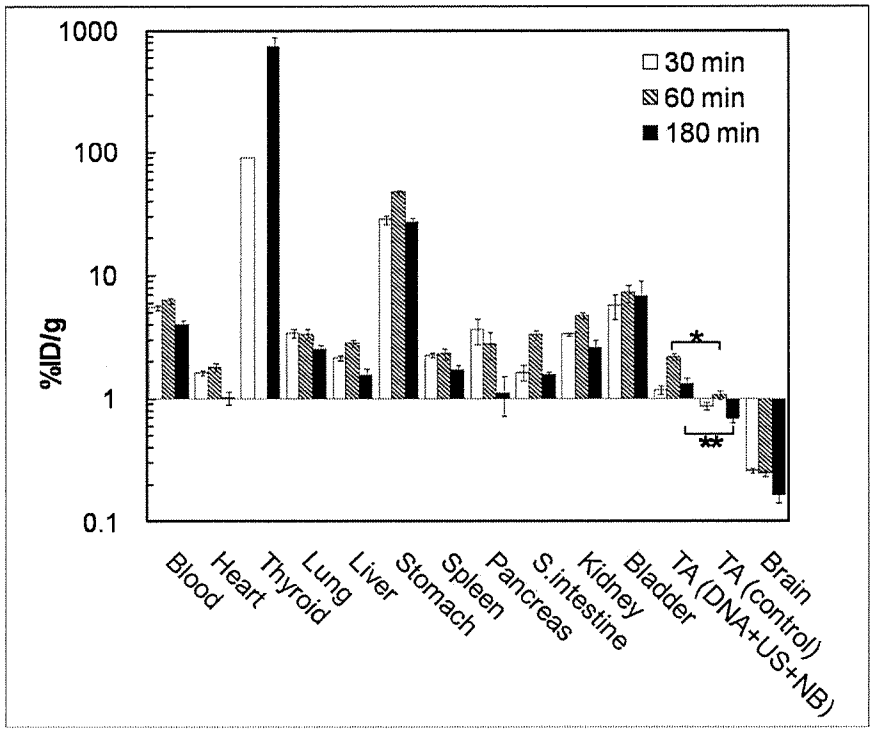
1000
100
10
1
0.1
%ID/g
30 min
60 min
180 min
*
**
Blood
Heart
Thyroid
Lung
Liver
Stomach
Spleen
Pancreas
S.intestine
Kidney
Bladder
TA (DNA+US+NB)
TA (control)
Brain

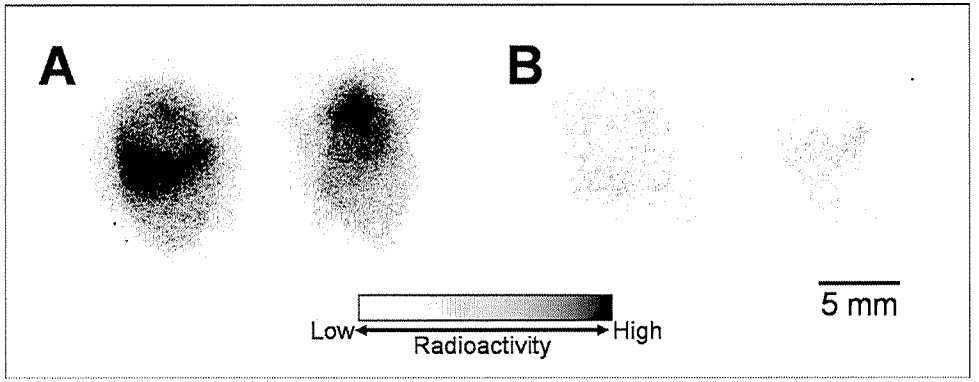
A
B
Low
High
Radioactivity
5 mm

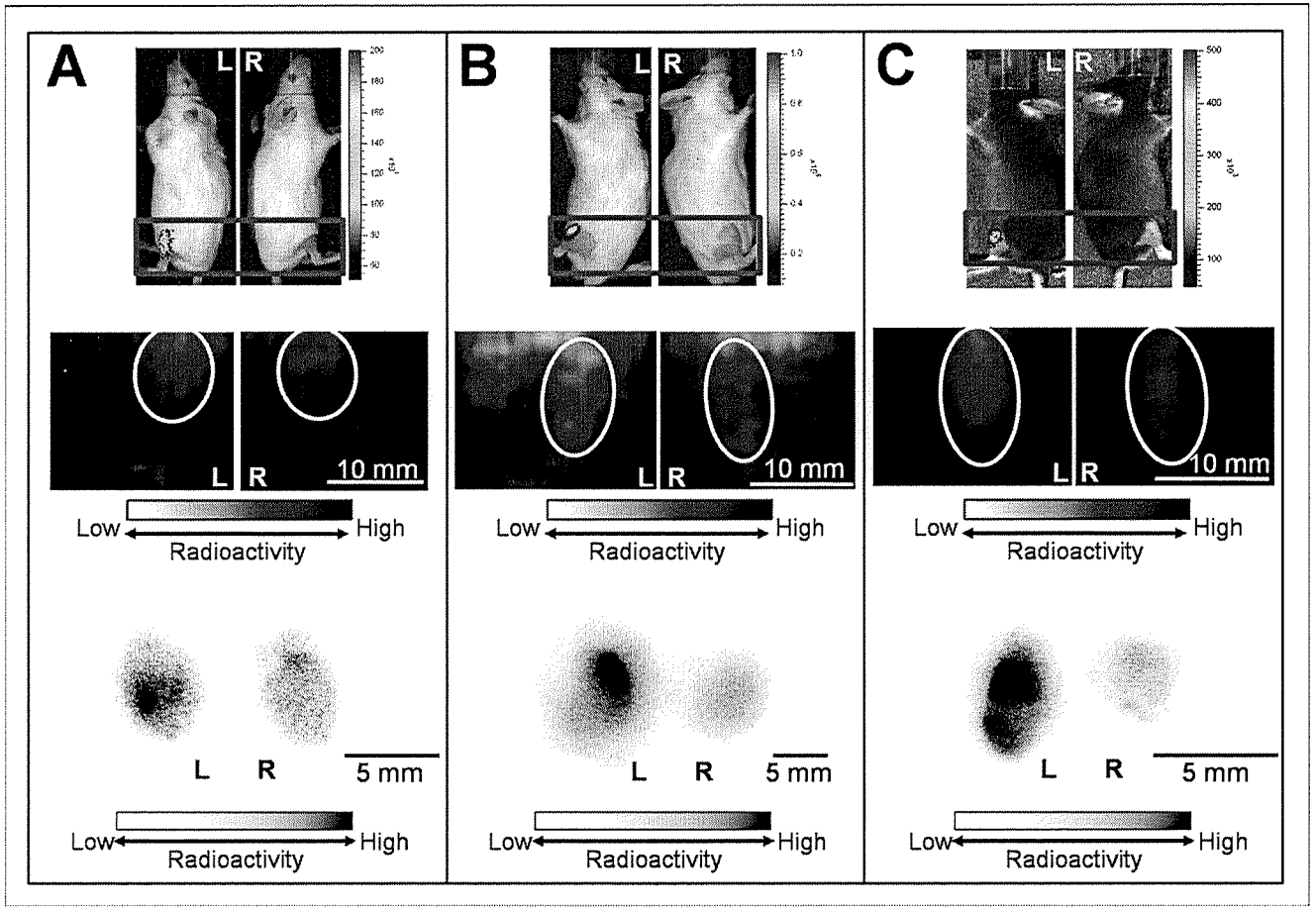
A
L
R
L
R
10 mm
Low
High
Radioactivity
L
R
5 mm
Low
High
Radioactivity
B
L
R
L
R
10 mm
Low
High
Radioactivity
L
R
5 mm
Low
High
Radioactivity
C
L
R
L
R
10 mm
Low
High
Radioactivity
L
R
5 mm
Low
High
Radioactivity

2009年11月10日発行（年4回2,5,8,11月）第10巻第4号（通巻48号） ISSN 1345-9031 CODEN：KIEGA2

Vascular Biology & Medicine Vol.10/No.4 2009.11

血管医学

特集

癌と血管―イメージングから治療まで

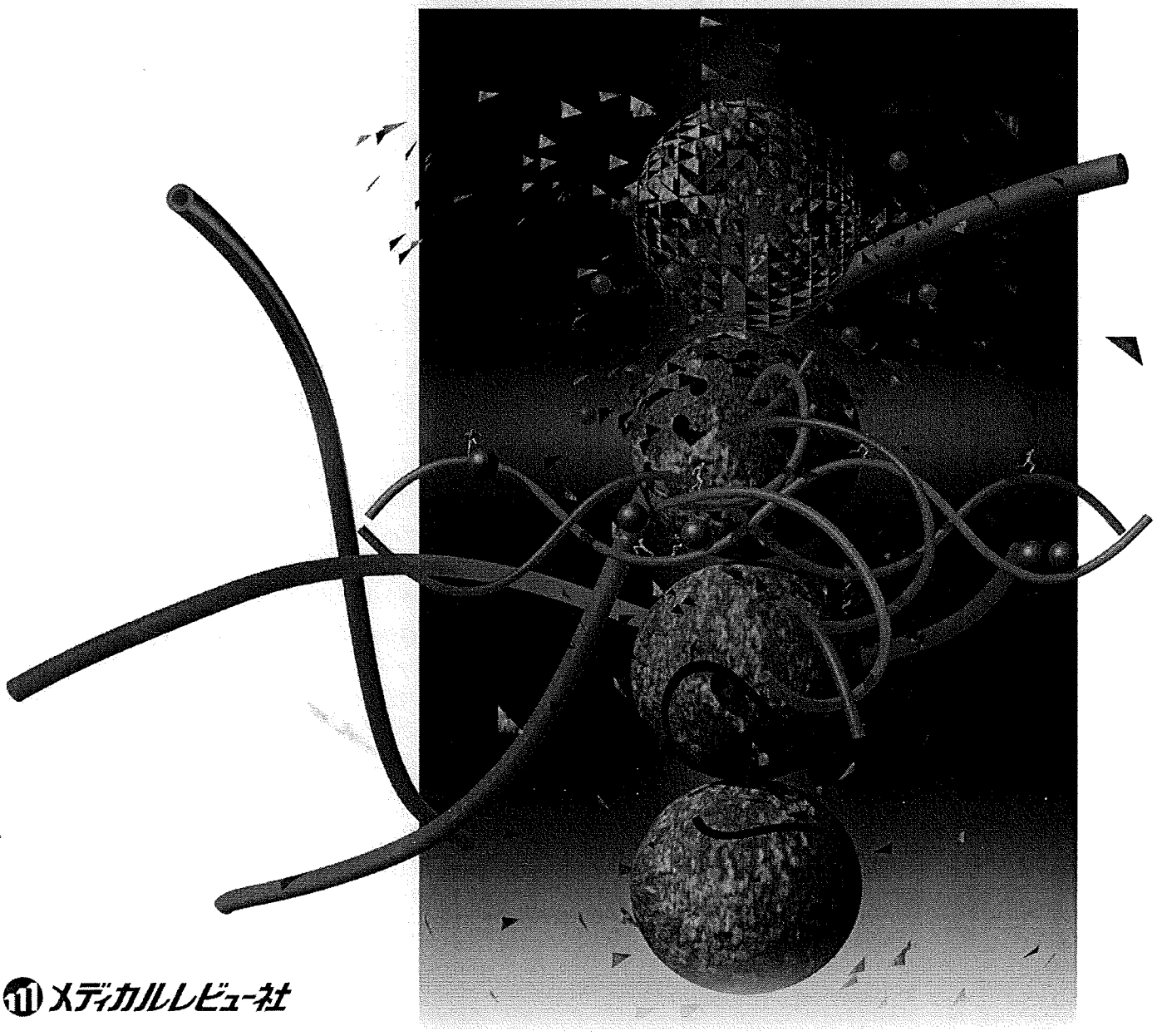

メディカルレビュー社